# Geocenter variations caused by atmosphere, ocean and surface ground water

D. Dong, J. O. Dickey, and Y. Chao
Jet Propulsion Laboratory, California Institute of Technology
M. K. Cheng
Center for Space Research
University of Texas at Austin

*"groundwater"
is one word.
Global for correction,*

**Abstract:** The geocenter variations reflect the global scale mass redistribution and the interaction between the solid Earth and the mass load. Determination of the geocenter variations due to surface mass load from various geophysical sources places constraints on the variations of the origin of terrestrial reference frame, and provides the expected range of variations for space-geodesy. Once the geocenter variations from satellite measurements and from the surface mass load contributors can be determined with sufficient accuracy, the residuals between the two will provide important constraints on the mass redistribution from various internal processes. Our results suggest that on the time scale from 30 days to 10 years the primary variability of geocenter variations from atmosphere, ocean and surface ground water occurs on the annual and semiannual scales. The lumped sum of these surface mass load induced geocenter variations is within 1 cm level.

## 1. INTRODUCTION

Global mass redistribution alters Earth rotation, produces temporal variations of the gravitational field, and shifts the position of geocenter, which is defined as the center of figure (CF) of the Earth relative to the center of mass (CM) of the Earth including mass load. Variation of the geocenter reflects the global mass balance and the interaction between the solid Earth and the mobile mass on the Earth. It also provides important constraints on the origin of the terrestrial reference frame. The satellite orbit is naturally related to the center of mass (CM), which remains static relative to an inertial frame in the case of no net external force for the whole Earth. Thus, geocenter variation can be monitored by the space-geodetic measurements.

Both the surface mass and the internal mass redistribution are capable of influencing the position of CF relative to CM. The internal mass redistribution are not directly observable, and can only be estimated from theoretical models. However, the surface mass redistribution can be estimated from either measurements or measurement constrained model simulations. Thus the estimated geocenter variations from surface mass redistribution provide constraints on the origin of the terrestrial reference frame, and could be directly compared with the space-geodesy

1

derived geocenter variations. Results will provide insight in₍ₕ₎ uncovering the sources of

geophysical mass redistribution and interpreting differences among various space-geodetic

analyses. In this paper, the contributions to geocenter variations from the surface loads, such

as atmospheric pressure, ocean and surface water are estimated and discussed.

## 2. THE TRAJECTORY OF CENTER OF FIGURE (CF) IN INERTIAL FRAME

Geocenter variations are related to the adopted reference frame, in particular for its

origin. Various Earth-related frames are utilized for different purposes. The origins of these

frames are usually defined as one of the three centers: the center of mass of the Earth + load

system (CM), the center of mass of the Earth without load (CE) and the center of figure of the

outer surface of the solid Earth (CF). When no external net forces acting on the Earth, CM will

stay static in an inertial frame. While CE and CF may change their positions as viewed in the

inertial frame due to mass redistribution. Without loss of generality we define an inertial frame

with CM as its origin and let the CM, CE and CF coincide in the case of no mass

redistribution. In this inertial frame the coordinates of CM, CE, CF and mass load are denoted

as $r_{CM}$, $r_{CE}$, $r_{CF}$ and $r_{load}$ respectively. We only consider the case without external net force,

where $r_{CM} = 0$ is always valid. Since the surface mass redistribution processes are generally

expressed in an Earth-fixed reference frame with CE as its origin (hereafter as CE frame), it is

convenient to use the coordinates of CF and mass load in this CE frame (defined as $\bar{r}_{CF}$ and

$\bar{r}_{load}$). There are simple geometric relations

$$r_{load} = r_{CE} + \bar{r}_{load}, \quad r_{CF} = r_{CE} + \bar{r}_{CF} \tag{1}$$

Mass balance leads to

$$M_e \, r_{CE} + M_l \, r_{load} = (M_e + M_l) \, r_{CE} + M_l \, \bar{r}_{load} = 0 \tag{2}$$

where $M_e$ and $M_l$ represent the mass of Earth (without load) and mass of load respectively.

Equations (2) and (1) indicate that the variations of $r_{CE}$ and $r_{CF}$ can be computed by the two CE

frame defined quantities $\bar{r}_{CF}$ and $\bar{r}_{load}$. In the CE frame, the mass load can be expressed in the

form of sum of spherical harmonics and only the degree one spherical harmonics of mass load

contributes to the $\bar{r}_{load}$ [*Trupin et al.,* 1992]. We denote the degree one surface mass load

density as

$$\Delta\sigma = c_z \cos\theta + c_x \sin\theta \cos\lambda + c_y \sin\theta \sin\lambda \tag{3}$$

where $c_x$, $c_y$, $c_z$ are spherical harmonics expansion coefficients, $\theta$ and $\lambda$ are colatitude and longitude respectively. Note that the $\bar{r}_{load}$ is the integral of the product of surface mass load and its position vector, only degree one spherical harmonics give non-zero integrals:

$$\bar{r}_{load} = \frac{a^3}{M_l} \int \Delta\sigma(\cos\theta\hat{e}_z + \sin\theta\cos\lambda\hat{e}_x + \sin\theta\sin\lambda\hat{e}_y)d\Omega = \frac{4\pi a^3}{3M_l}\left(c_x\hat{e}_x + c_y\hat{e}_y + c_z\hat{e}_z\right) \quad (4)$$

where a is the mean radius of the Earth.

First we discuss the simplest case in which the Earth's deformation is neglected. In this case, the Earth's shape is unchanged. The degree one mass load does not produce the torque and does not change the momentum, both lead to a rigid rotation. Thus only rigid translation motion is allowed which is invisible in the CE frame. $\bar{r}_{CF}$ keeps unchanged before and after the mass loading which is set to zero because CE and CF are coincided before mass loading. From (1) and (2),

$$r_{CF} = r_{CE} = -\frac{M_l}{M_e + M_l}\bar{r}_{load} \quad (5)$$

For a deformable Earth, the displacements of the surface are characterized by the degree one load Love number. However, for the degree one mass load, the three boundary conditions for solving the three degree one mass load Love number ($k_1$, $h_1$, $l_1$) become dependent, an arbitrary rigid shift solution can be added without violating the boundary conditions and only two linear combinations of the $k_1$, $h_1$, $l_1$ can be resolved [*Farrell*, 1972; *Dahlen*, 1976]. *Farrell* [1972] and *Dahlen* [1976] used the CE frame and constrained the rigid shift solution by forcing the degree one gravitational potential to be zero in the inertial frame (equivalent to $k_1 = 0$ in the CE frame). Their derived degree one load Love numbers are related to the CE frame and can be used to compute the $\bar{r}_{CF}$. If the $\bar{r}_{load}$ is unchanged during the deformation, the $r_{CE}$ will be the same as computed from (5). While $\bar{r}_{CF}$ is no longer to be zero as derived by *Trupin et al.* [1992] (assuming $M_l \ll M_e$):

$$\bar{r}_{CF} = \frac{4\pi a^3}{3M_e}\frac{h_1 + 2l_1}{3}\left(c_x\hat{e}_x + c_y\hat{e}_y + c_z\hat{e}_z\right) = \frac{h_1 + 2l_1}{3}\frac{M_l}{M_e}\bar{r}_{load} \quad (6)$$

$$r_{CF} = -(1 - \frac{h_1 + 2l_1}{3})\frac{M_l}{M_e + M_l}\bar{r}_{load} \quad (7)$$

where Trupin *et al.* [1992] expressed (7) in terms of CM relative to CF (just opposite sign). Using the values of $h_1 = -0.290$ and $l_1 = 0.113$ [*Farrell*,1972], formula (7) indicates that the deformation slightly enlarges the amplitude of $r_{CF}$ by about 2.1% in the inertial frame.

3

The assumption of unchanged $\bar{r}_{load}$ will cause somewhere disconnection and somewhere mixing between the mass load and its underneath surface of the Earth after the deformation. A modified assumption presumes that the mass load is stuck on its underneath deformed surface of the Earth. We get

$$\bar{r}_{load}(\text{after deformation}) = (1 + \frac{M_l}{M_e}\frac{h_1+2l_1}{3}) \bar{r}_{load}(\text{before deformation}) \qquad (8)$$

Since the mass load is typically much smaller than the mass of the Earth, the influence of the deformation on $\bar{r}_{load}$ is so small that the $r_{CF}$ still can be computed from (7) using $\bar{r}_{load}$(before deformation) to the first order approximation. In this case, the $r_{CE}$ will change its position slightly in the inertial frame due to the deformation.

$$r_{CE} = -\frac{M_l}{M_e+M_l}(1 + \frac{M_l}{M_e}\frac{h_1+2l_1}{3}) \bar{r}_{load}(\text{before deformation}) \qquad (9)$$

Formula (9) indicates that the deformation slightly reduces rather than enlarges the amplitude of $r_{CE}$ in the inertial frame. Thus the deformation functionally separates CE and CF (for the modified assumption, the deformation even makes CE and CF move towards opposite* *See below* direction) as viewed in the inertial frame. Such an apparent discrepancy stems from the structure of the Earth for $r_{CF}$ only related to the surface of the Earth while $r_{CE}$ concerns the whole Earth. In a homogeneous Earth, $h_1(r) + 2l_1(r) = 0$ [*Fang* 1996, personal *This* communication], therefore $r_{CF}$ always coincides with $r_{CE}$ and such a discrepancy disappears. *Ref is* For a radially layered Earth this discrepancy implies that somewhere beneath the surface of the *not on* Earth, $h_1(r) + 2l_1(r)$ should change its sign from negative to positive. *Fang and Hager* [1997] *the list.* calculate various degrees of load Love numbers and their radial distributions based on the PREM model. Their results of the degree one load Love numbers (at the Earth's surface, $h_1 = -0.2846$, $l_1 = 0.1060$) confirm that at about 3170 km beneath the Earth's surface, the $h_1(r) + 2l_1(r)$ does change its sign from negative to positive. We do not discuss further modified assumptions, such as allowing the mass load to deform along with the surface, which is probably necessary in the ice sheet loading problems. However, it is unlikely to change the above geocenter variation discussion qualitatively.

Theoretically, both $r_{CF}$ and $r_{CE}$ can be used to describe the "geocenter variations". In practice, however, $r_{CF}$ is generally adopted since our terrestrial reference frame is defined and maintained by a set of tracking stations on the surface of the Earth. If the terrestrial tracking network has sufficient sites with global coverage, the satellite measured network translation relative to CM (or equivalent the perturbation of degree one Stokes coefficients) is a good

?

* the opposite direction
or
towards opposite directions 4

representation of $r_{CF}$ [*Vigue et al.*, 1992; *Watkins and Eanes*, 1993]. In the following sections, we use $r_{CF}$ to characterize the "geocenter variations".

### 3. GEOCENTER VARIATIONS INFERRED FROM SURFACE MASS LOAD

3.1 Atmosphere

Surface pressure data, sampled twice a day and girded by 2.5°x2.5°, from the European Center for Medium-range Weather Forecasts (ECMWF) and from the National Meteorological Center (NMC) were used to calculate their first degree spherical harmonics. For the variations with time scale longer than one month, inverted barometer (IB) model is a good approximation for the oceanic response to surface air pressure [*Ponte et al.*, 1991; *Ray and Cartwright*, 1994]. In this paper, ECMWF land-ocean mask was adopted to calculate the IB effect for both ECMWF and NMC data. The ECMWF/WMO series, spanning from 1980 to 1989, used initialized analysis., While the ECMWF/TOGA series, spanning from 1986 to 1994, were from uninitialized analysis. The normal mode initialization scheme was used to suppress the initial transients in the mass and wind field to improve the numerical weather predictions with the fast modes (period less than 48 hours) being primarily influenced modes [*Rasch*, 1985; *Wergen*, 1989]. At the four year overlapped period (1986-1989), we calculated the differences of geocenters inferred from the first degree spherical harmonics of the two ECMWF series. As expected, that the differences between the two series are primarily a constant bias and high-frequency components (period 1-5 days) with small amplitudes (corresponding to high-frequency geocenter variation less than 0.2 mm). Thus for the study at seasonal and interseasonal time scales we simply connect the two series at the end of 1989 with the constant biases adjusted and repaired. Improvements in the analytical models have led to occasional step-like discontinuities in both NMC and ECMWF data derived harmonics series, but at different epochs. These step-like discontinuities have been removed by adding a constant value determined from the misfit between the smoothing spline values before and after the step using the NMC-ECMWF difference series. The corresponding geocenter variations were calculated from (7). To focus on the seasonal, intraseasonal and interseasonal time scales, both NMC and ECMWF data derived geocenter variation series were filtered with band-pass period from 30 days to 10 years. Fig. 1 plots the resultant atmosphere induced geocenter variations from ECMWF series (01/80-12/94) and NMC series (01/84-08/93). We use the scatters of the two series from their average to characterize the self-consistencies of the atmosphere derived geocenter variation series. The estimated scatters for x, y, z coordinates are 0.08 mm, 0.14 mm and 0.29 mm respectively. Both visual comparison and the estimated scatters demonstrate that the two series is in good agreement. The variation patterns showed in Fig. 1 are likely dominated by seasonal signals with the caveat of that assuming both NMC and ECMWF series

5

have no significant common systematic errors. The largest estimated scatter is in z-component, reflecting the sparse measurements in polar region. Spectrum analyses using ECMWF data derived geocenter variation series indicate that the primary components are annual and semiannual components for all x, y, z series. The y series has the largest annual component (amplitude = 1.6 mm) and the z series has the largest semiannual component (amplitude = 0.9 mm). The y series show the most regular pattern with the amplitude of about 2 mm. While x series have only 1 mm amplitude, about half of the y series. Such a difference between x and y series reflects the land-ocean distribution. On the Earth, the ocean distribution is closer to the x-axis direction [*Lambeck* 1980], therefore the atmospheric mass redistribution over the ocean region is largely compensated by the IB effects.

## 3.2 Ocean

In the ocean, there are not enough data to calculate the currents and corresponding mass redistribution. The global 4-dimensional oceanic analysis, similar to the atmospheric analysis from NMC and ECMWF, is still not available yet. In this study, simulations from two ocean general circulation models (OGCM) forced with real-time NMC wind analysis were used. By using two models with completely different formulations, we hope to gain more confidence in the model simulations. One model uses depth as the vertical coordinate and is based on the modular ocean model (MOM) formulation [*Pacanowski et al.*, 1993]. The other model, however, uses density as the vertical coordinate [*Hu and Chao*, 1996], and is often referred to as isopycnal models (ISO hereafter). Both models are configulated over the global ocean from 80°S to 80°N. The horizontal resolution is 2° in longitude and 1° in latitude. There are 22 vertical levels for MOM and 11 layers for ISO. The continent-ocean boundary and ocean bottom topography are taken from realistic digital databases. At lateral walls a no-slip boundary condition is applied and no flux of heat and salt is allowed. Both models were first spin-up for 10 years forced by the climatological monthly wind with the initial condition by the Levitus [1982] January temperature and salinity distribution with zero currents. Then the wind stress from 1992 to 1994 was imposed from the daily wind obtained from the NMC 1000-mbar analysis. There are some adjustments during the first month switching from the climatological forcing to real-time forcing. We use the model results after February 1992. Since both models conserve the volume rather than the mass of the ocean, the total mass of ocean from individual solutions varies. If we take the simplest assumption of that the total mass variation is uniformly distributed into each oceanic grid, such an apparent variation of total mass of ocean can be remedied by a global scaling factor. Note that the mass center of ocean is calculated by (4), in which the total mass of ocean ($M_l$) is used to scaling the coordinates. Thus the global scaling for mass conservation of the whole ocean is automatically

realized in (4). To be consistent with the atmosphere results, the geocenter variation series from oceanic mass redistribution were band-pass filtered with the same cutoff periods. The resultant series, shown in Fig.2, indicates that the x, y, z series from ISO and MOM are in good agreement, but the differences are somewhat larger than that from ECMWF and NMC analyses. This is mainly because no oceanic data has been used to constrain the ocean model simulation. It is expected the difference between these two models will be reduced when assimilating in situ and satellite oceanic observations. The scatters from the averaged x, y, z series are 0.36 mm, 0.28 mm and 0.19 mm respectively. The ocean has the biggest contribution in the x component mostly due to the global land-ocean distribution. Spectrum analyses of the ISO series indicate that only the annual and semiannual components of x series (amplitude = 1.05 mm, 0.39 mm), the semiannual component of y series (amplitude = 0.29 mm) are above the scatter level. and

The annual and semiannual ocean tides ($S_a$, $S_{sa}$) also produce surface mass redistribution on the seasonal time scale. Considering that the satellite geodesy-derived ocean tide models, as well as the Schwiderski's $S_{sa}$ ocean tide model contain the contributions from other sources such as the atmospheric mass variations [*Dong et al.*, 1996], we use a self-consistent equilibrium ocean tide model [*Ray and Cartwright*, 1994] to calculate the ocean tide load and its corresponding geocenter variations. Since the signals are purely annual and semiannual, no band-pass filtering is needed. Geocenter variations are then calculated by (7). $S_{sa}$ ocean tide produces 0.36 mm, 0.03 mm, 0.36 mm semiannual components for x, y, and z series respectively. $S_a$ ocean tide produces 0.06 mm, 0.005 mm, 0.06 mm annual components for x, y, and z series respectively. The corresponding geocenter variation series are plotted in Fig. 3. Note that the y components from the equilibrium ocean tide are much smaller than the x components due to the joint contribution of the second degree zonal tidal potential and the ocean function.

3.3 Global surface water

The surface water redistribution was computed based on the procedures given by *Lei & Gao* [1992]. In brief, all land was divided into 683 square areas in approximately 5 degree by 5 degree based on river basins in order to estimate water storage loads. The monthly precipitation and temperature at each grid area are obtained from a surface spherical harmonics interpolation using the monthly mean precipitation and temperature data from about 1200 stations over the world. The runoff coefficients of a grid is taken from the map of runoff coefficients of the rivers published by UNESCO [1977], the evaporation at a grid area is computed based on the results given by *Van Hylkama* [1970] and *Lamb* [1972]. The surface water storage in each grid is calculated based on the commonly used assumptions discussed by

*Hinnov and Wilson* [1987], *Chao et al.* [1988]. In our computation, the precipitation is considered to be in the form of snow or ice when the temperature falls belong zero and there is no runoff. The uncertainty, largely due to the very sparse station coverage and adopted models, of the calculated surface water Stokes coefficient series can not be assessed directly. Detailed comparison is given by *Cheng et al.* [1997]. The degree one Stokes coefficient series were used to calculate the corresponding geocenter variation series. To be consistent with other series, these groundwater induced geocenter variation series were band-pass filtered with the same cutoff periods and were plotted in Fig. 4. Spectrum analyses indicate that the groundwater mass redistribution are dominated by annual variations for all x, y, and z series with corresponding amplitudes are 3.28 mm, 2.94 mm, 3.57 mm for annual components and 0.84 mm, 0.94 mm, 0.66 mm for semiannual components respectively. Using the RAND data set of the global snow depth [*Schutz and Bregman*, 1988], the estimated contribution from snow to the annual geocenter variation in z component is 2.2 mm. These results indicate that the ice and snow redistribution in the polar region makes significant contributions to the geocenter variations in z component.

3.4 Melting glaciers and sea level

Glacier melting and sea level change due to global mass balance also contribute to the geocenter variations. Using yearly mass balance data of glaciers and yearly averaged tide gauge data, *Trupin et al.* [1992] calculated the contributions from melting glaciers and sea level to the geocenter variations. The seasonal and intraseasonal geocenter variations were not resolved due to the resolution limitation of the yearly averaged data. Their results revealed millimeter level secular trend and sub-millimeter level interannual variations of the geocenter displacements. Although the calculated interannual geocenter variations were considered insignificant compared with the data noise level, the contributions from changes of glaciers and sea level to the geocenter variations from intraseasonal to interannual time scales are probably not negligible compared with other contributors and should be quantitatively evaluated once the higher resolution data are available.

## 4. CONCLUSIONS

CE is used by many theoretical models, such as the Earth tide model, and the calculation of the mass load Love number. The origin of our terrestrial reference frame is determined and maintained by a set of tracking stations, and therefore corresponds to CF. Satellite measured network shift of a global terrestrial network reflects the trajectory of CF in an inertial frame, which is usually described as the "geocenter variation". Mass redistribution on the Earth shifts both CE and CF from CM. Deformation of the layered solid Earth under surface mass load

further separates CF and CE from their positions of without deformation. The geocenter variations reflect the global scale mass migration and the interaction between solid Earth and mass load. Determination of the geocenter variations due to surface mass load from various geophysical sources places constraints on the variations of the origin of terrestrial reference frame, provides a range of the CF variation spectrum for space-geodesy. Once the geocenter variations from satellite measurements and from the surface mass load contributors can be determined with sufficient accuracy, the residuals between the two will provide important constraints on the mass redistribution from various internal processes. Our results suggest that on the time scale from 30 days to 10 years the primary variability of geocenter variations from atmosphere, ocean and surface ground water occurs on seasonal time scales. The annual and semiannual components of geocenter variations from various surface mass load are listed in Table 1 and plotted in Fig. 5, which display the observed geocenter variations and the lumped sum from multiple contributors. Ground water is the largest contributor to all three components at the annual period and both x and y components at the semiannual period. The atmosphere is the largest contributor for the semiannual z component with ground water being about 25% less. Unfortunately, the mass redistribution of the surface ground water is the least understood one and deserves substantial study. The total annual terms (see Table 1) are considerably larger than the corresponding semiannual terms (see Table 1) by a factor of 8.1, 8.3, 2.7 for x, y, z components respectively. Note the different scales in Figure 5. Although there are difficulties to directly assess the uncertainties of these time series, the x, y components of geocenter variations from seasonal to interannual time scales are likely within 1 cm level unless these time series have significant errors, or we have not included some important surface mass load contributors, or the internal mass redistribution processes play a dominant role. Melting glaciers and sea level change, which were not quantitatively assessed in this paper, could make a significant contribution to the z component of geocenter variations (see Fig. 5 of *Trupin et al.*, 1992). If a single satellite has sufficient measurements and allows the estimation of the geocenter variations together with higher degree, saying to 4x4, Stokes coefficients (assuming the unmodeled effects of other parameters, such as the once per revolution parameter, are negligible), then the estimated geocenter variations can be compared with our results. Otherwise the single satellite determined perturbations of the degree one Stokes coefficients are actually the linear combinations of degree one and other degree Stokes coefficients [*Kar*, 1996]. To perform the comparison with such single satellite determined perturbations of the degree one Stokes coefficients, the same linear combinations of Stokes coefficients from various surface mass load series must be formed. Multiple satellite analysis will break the linear combination and make the comparison of the estimated geocenter variation

9

series with our derived geocenter variation series possible [*Watkins and Eanes*, 1993; *Kar*, 1996].

**References:**

Chao, Y. and W. P. O'Connor, Global surface-water-induced seasonal variations in the Earth's rotation and gravitational field, *Geophys. J.*, 94, 263-270, 1988

Chao, Y. and L. L. Fu, A comparison between the TOPEX/POSEIDON data and a global ocean general circulation model during 1992-1993, *J. Geophys. Res.*, 100, 24965-24976, 1995

Cheng, M. K., et al., Observed seasonal variations in the Earth's gravity field, in preparation, 1997

Dahlen, F. A., The passive influence of the oceans upon the rotation of the Earth, *Geophys. J. R. astro, Soc.*, 46, 363-406, 1976

Dong, D., R. S. Gross, and J. O. Dickey, Seasonal variations of the Earth's gravitational field: an analysis of atmospheric pressure, ocean tidal, and surface water excitation, *Geophys. Res. Lett.*, 23, 725-728, 1996

Fang, M. and B. H. Hager, Energy load Love numbers, in preparation, 1997

Farrell, W. E., Deformation of the Earth by surface loads, *Reviews of Geophysics and Space Physics*, 10, 761-797, 1972

Hinnov, L. A., and C. R. Wilson, An estimate of the water storage contribution to the excitation of polar motion, *Geophys. J. R. astro. Soc.*, 88, 437-459, 1987

Hu. D., and Y. Chao, Upper ocean variabilities during 1992-93: simulations with global isopycnal and Cartesian coordinate ocean models versus observations, *submitted to J. Geophys. Res.*, 1996

Kar, S., Long-term variations in the geocenter observed from laser tracking of multiple earth satellites, Ph. D Thesis, University of Texas at Austin, 1996

Lamb, H. H., *Climate: Present, Past and Future*, Methuen, London, 1972

Lambeck, K., The Earth's variable rotation, *Cambridge University Press*, 1980

Lei, X. P. and B. X. Gao, The excitation of water storage distribution and the annual wobble, *Acta Astronomica Sinica*, 33, 61-66, 1992

Levitus, S., Climatological Atlas of the world ocean, *NOAA Prof. Pap.* 13, 173 pp, Silver Spring, MD, 1982

Pacanowski R., K. Dixon, and A. Rosati, Modular ocean model users guide, *Ocean Group Tech. Rep. 2.*, NOAA Geophysical Fluid Dynamics Laboratory, Princeton, New Jersey, 1991

Ponte, R. M., D. A. Salstein, and R. D. Rosen, Sea level response to pressure forcing in a barotropic numerical model, *J. Phys. Oceanogr.*, 21, 1043-1057, 1991

Rasch, P. J., Developments in normal mode initialization, part II: a new method and its comparison with currently used schemes, *Monthly Weather Review*, 113, 1753-1770, 1985

Ray, R. D., and D. E. Cartwright, Satellite altimeter observations of the Mf and Mm ocean tides, with simultaneous orbit corrections, in *Gravimetry and Space Techniques Applied to Geodynamics and Ocean Dynamics*, edited by B. E. Schutz, A. Anderson, C. Froidevaux, and M. Parke, pp. 69–78, American Geophysical Union Geophysical Monograph 82, IUGG Volume 17, Washington, D.C., 1994.

Schutz, C., and L. D. Bregman, Global annual snow accumulation by months, N-2687-RC, February, 1988

Trupin, A. S., M. F. Meier, and J. M. Wahr, Effects of melting glaciers on the Earth's rotation and gravitational field: 1965-1984, *Geophys. J. Int*, 108, 1-15, 1992

*Please check. Is it really Trupin, or is it Turpin?*

11

Van Hylkama, T. E. A., Water balance and Earth unbalance, Proc. Reading Symposium on World Water balance, 92, 434-444, 1970

Vigue, Y, S. M. Lichten, G. Blewitt, M. B. Heflin, and R. P. Malla, Precise determination of Earth's center of mass using measurements from the Global Positioning System, *Geophys. Res. Lett.*, 19, 1487-1490, 1992

Watkins, M. M. and R. J. Eanes, Long-term changes in the Earth's shape, rotation and geocenter, *Advances in Space Research,* 13(11), 251-255, 1993

Wergen, W., Normal mode initialization and atmospheric tides, *Quart. J. Roy. Meteo. Soc.,* 115, 535-545, 1989

World water balance and water resources of the Earth's, UNESCO, 1977, Paries

Table 1. Annual and semiannual geocenter variations from surface mass redistributions

| source* | | Annual | | Semiannual | |
|---|---|---|---|---|---|
| | | Amp+. (mm) | Phase+ (deg.) | Amp+. (mm) | Phase+ (deg.) |
| | x | 0.67 | 284.1 | 0.28 | 270.4 |
| Atmosphere | y | 1.60 | 270.7 | 0.46 | 36.8 |
| | z | 1.06 | 312.8 | 0.89 | 90.7 |
| | x | 1.05 | 258.8 | 0.39 | 67.7 |
| Ocean non-tidal | y | 0.09 | 301.0 | 0.29 | 101.9 |
| | z | 0.18 | 37.7 | 0.16 | 220.6 |
| | x | 0.06 | 87.6 | 0.36 | 290.8 |
| Ocean tide | y | 0.01 | 267.6 | 0.03 | 110.8 |
| | z | 0.06 | 267.6 | 0.36 | 110.8 |
| | x | 3.28 | 219.8 | 0.84 | 169.4 |
| Ground water | y | 2.94 | 19.6 | 0.94 | 258.2 |
| | z | 3.57 | 55.2 | 0.66 | 13.,6 |

\* ECMWF data are used for atmosphere. Isopycnal ocean circulation model is used for ocean non-tidal. Self-consistent equilibrium Sa and Ssa tide models are used for ocean tide.

+ Amplitude A and phase $\phi$ are defined by $A\sin[\omega(t-t_0)+\phi]$ where $t_0$ is January 1, 1990, $\omega$ is the frequency.

FIGURE CAPTIONS:

Figure 1:    Geocenter variation from our extended ECMWF series (solid line) and NMC series (dashed line). ECMWF land-ocean mask was used in the inverted barometer (IB) model. Both series passed band-pass filtering with the cutoff period from 30 days to 10 years.

Figure 2:    Geocenter variation from isopycnal model (solid line) and modular ocean model (dashed line). Both series passed band-pass filtering with the cutoff period from 30 days to 10 years.

Figure 3:    Geocenter variation from equilibrium Ssa tide (solid line) and Sa (dashed line). A self-consistent equilibrium ocean tidal model [*Ray and Cartwright,* 1994] was used.

Figure 4:    Geocenter variation from surface groundwater series [*Cheng,* 1997]. The series passed band-pass filtering with the cutoff period from 30 days to 10 years.

Figure 5:    Annual (first row) and semiannual (second row) components of geocenter variation. Note the scales of the two rows are different. The notations of contributors are: A atmosphere, O ocean current, T ocean tide, W surface groundwater. The phase is referred to Jan. 1 with sine convention.

14
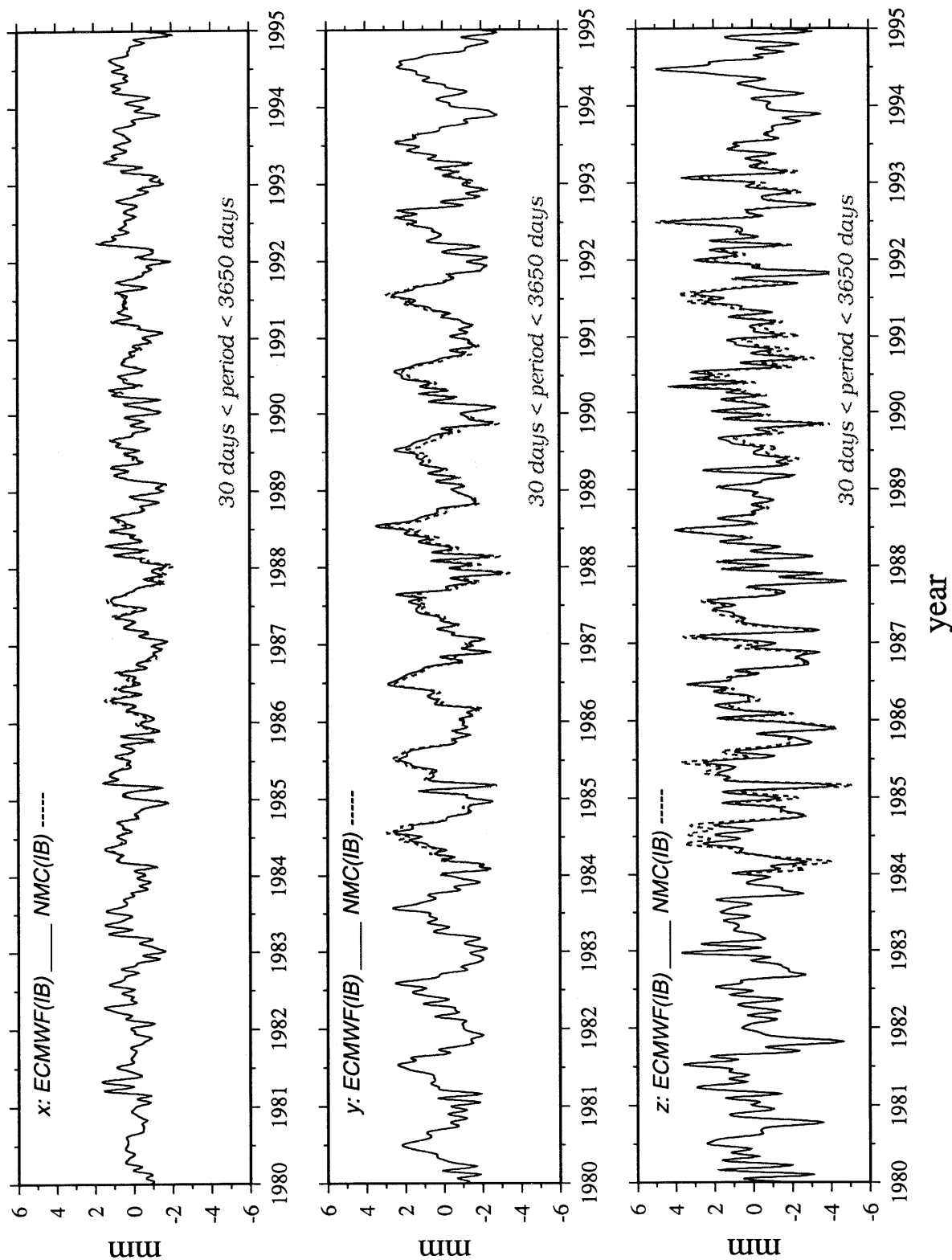
Fig. 1  Geocenter variation from air mass (01/80 - 12/94)
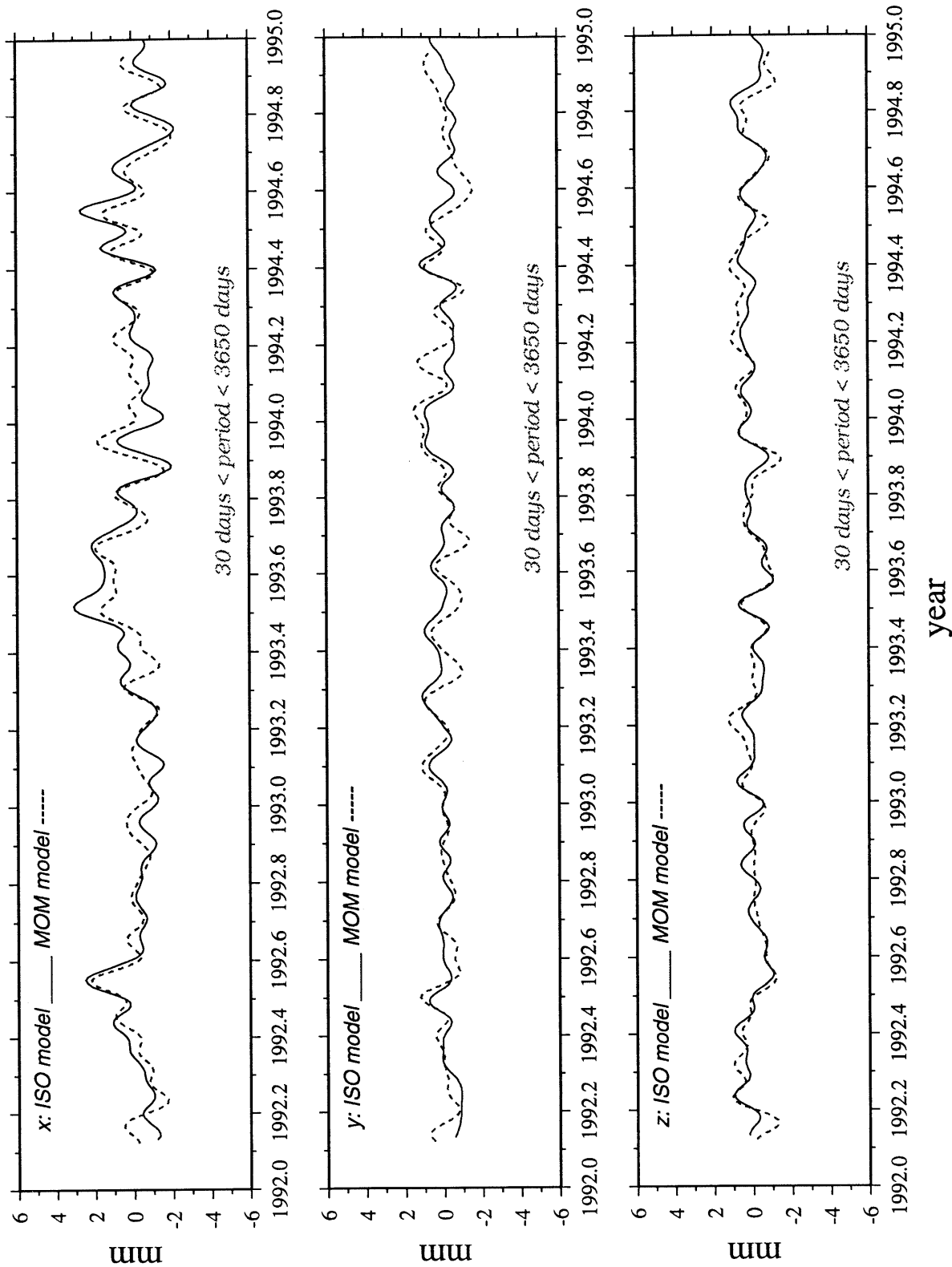
Figures are labeled
not numbered

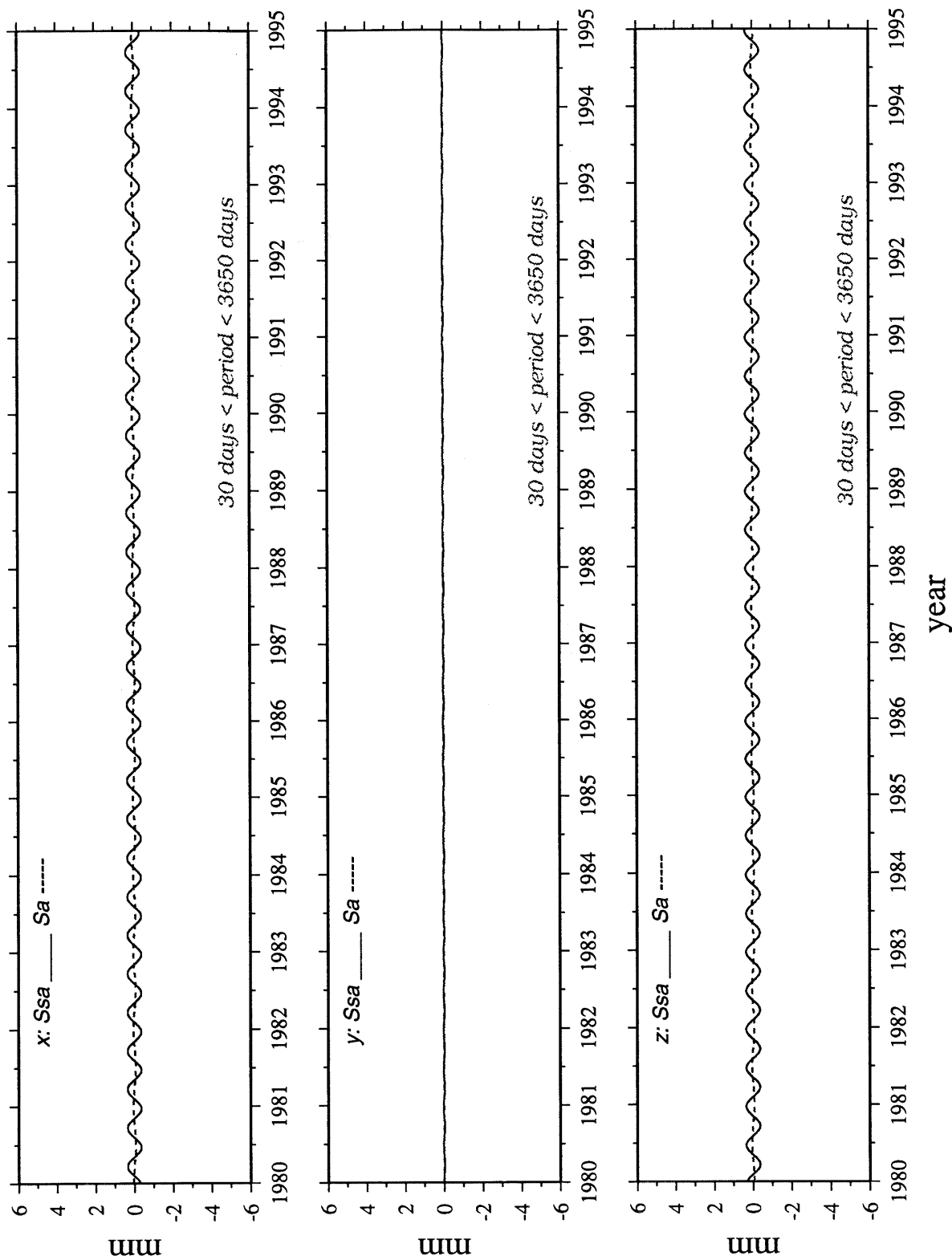Fig. 2    Geocenter variation from ocean mass (02/92 - 12/94)

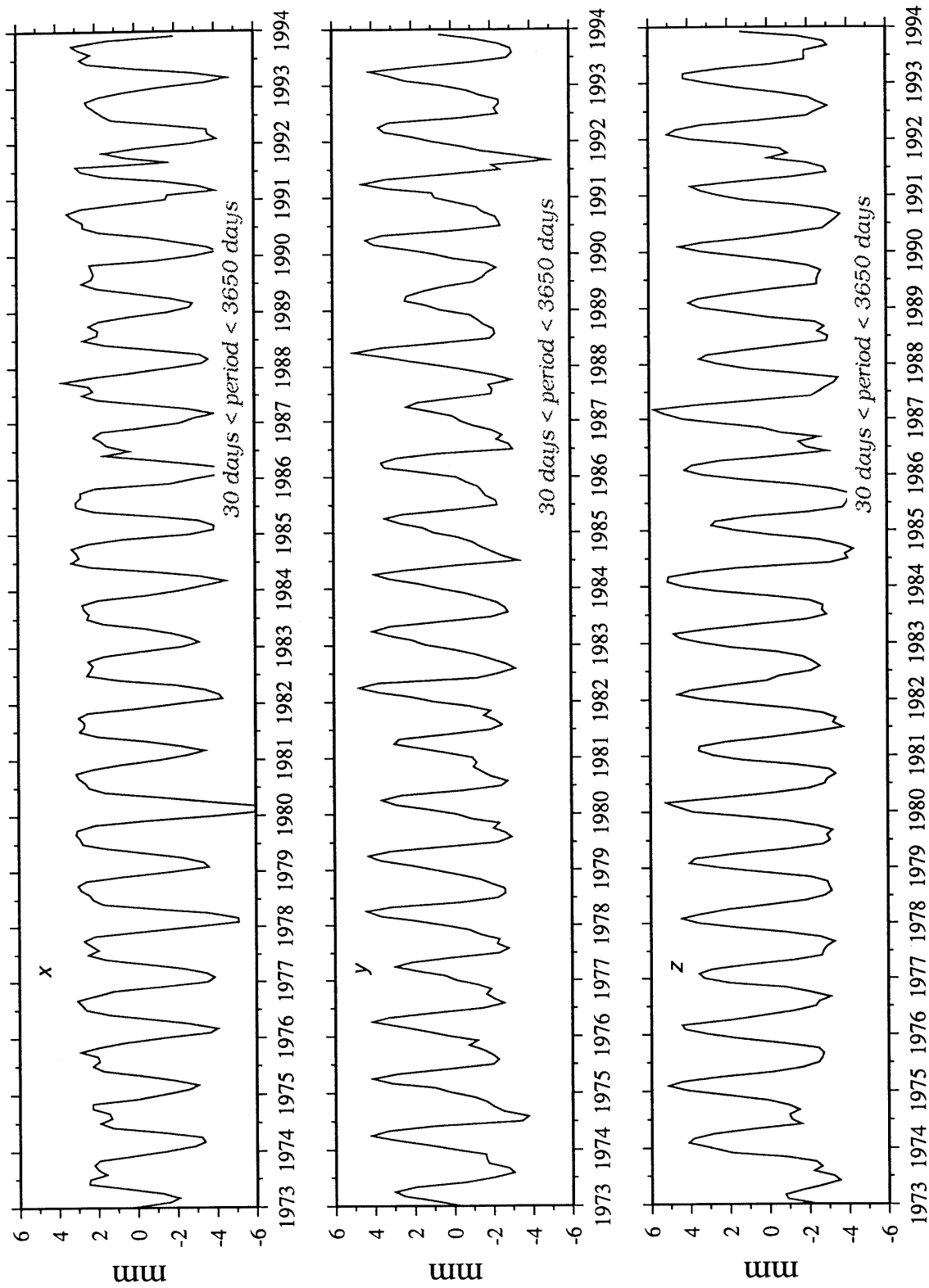Fig. 3    Geocenter variation from ocean tide (01/80 - 12/94)

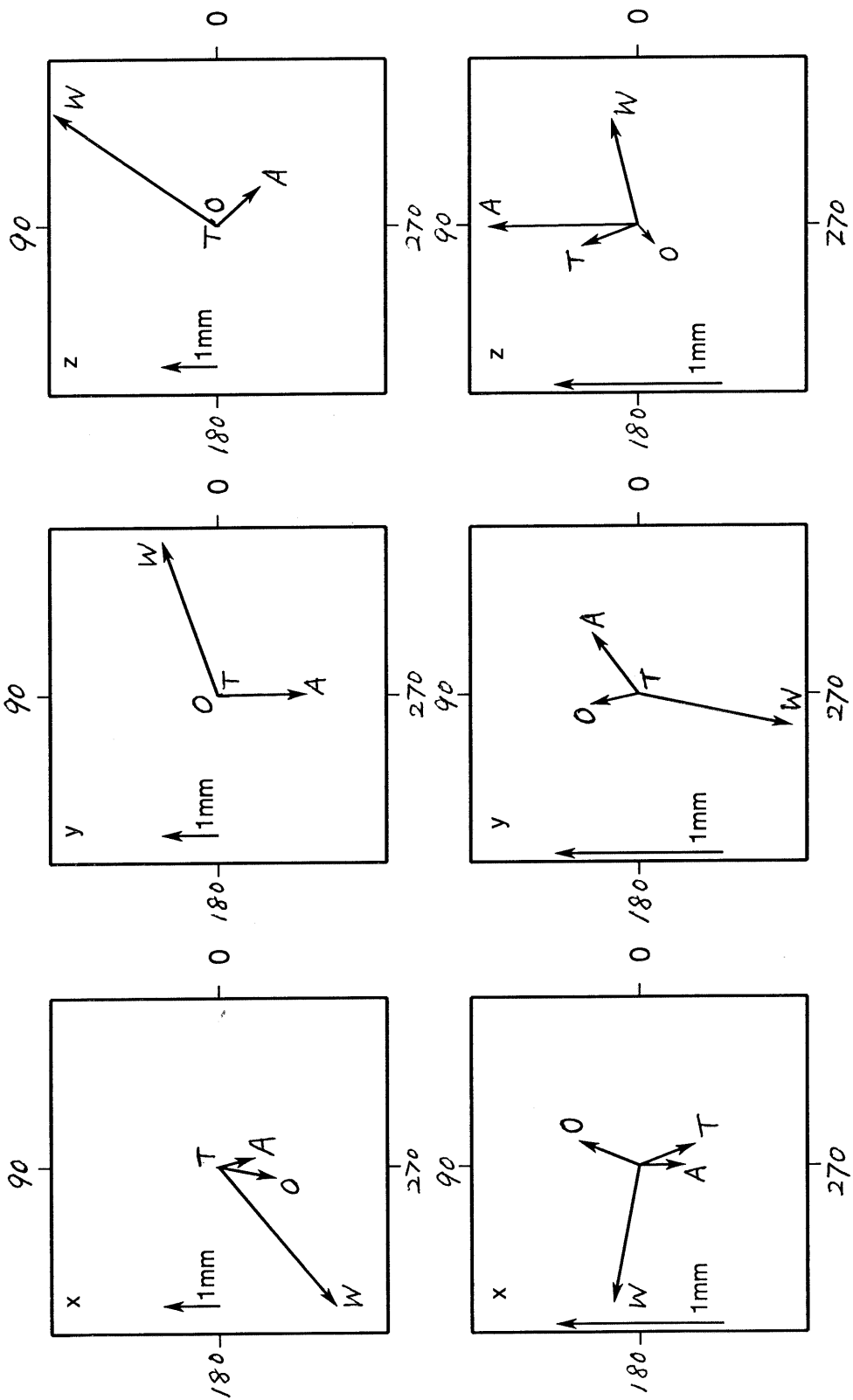Fig. 4. Geocenter variation from groundwater (01/73 - 12/93)

Fig. 5